Multiphysics Simulation of Aluminium Electrolysis Cells for Renewable Energy Consumption

Jie Li[1], Shenzhou Li[2], Hongliang Zhang[3], Jiaqi Li[4], Can Chen[5] and Zhong Zou[6]
1, 3, 6. Professor
4. Assistant Research Fellow
2, 5. Doctor of Philosophy
School of Metallurgy and Environment – Central South University, Changsha, China
Corresponding author: csu13574831278@csu.edu.cn
https://doi.org/10.71659/icsoba2025-al070

Abstract

Worldwide the aluminum electrolysis industry faces significant challenges in energy conservation, emission reduction, and environmental protection. Utilizing renewable electricity is expected to become one key pivotal solution for decarbonizing primary aluminum production. This study establishes a transient electro-thermal coupled solidification model for aluminum electrolysis cell to investigate the thermal balance instability induced by current variations during the integration of renewable energy sources. By simulating various fluctuating current conditions, the study analyzes the distribution of the temperature field within the electrolysis cell and the variations in the morphology of the cell sidewall ledge are analyzed. Additionally, the study explores the influence of different process parameters on the morphology of the cell sidewall ledge and proposes a control strategy for mitigating the effects of current variations. The results indicate that the current insulation structure of the electrolysis cell can effectively self-regulate current variations within a range of ±5 %. However, relying solely on the inherent thermal balance of the cell to current variations exceeding ±15 % poses significant operational risks. Under fluctuating current conditions, the morphology of the cell sidewall ledge can be controlled by adjusting process parameters, specifically: MgF_2 content of 2.5–3.5 wt.%, CaF_2 content of 4–8 wt.%, Al_2O_3 content of 2–3 wt.%, cryolite ratio (CR) of 2.3–2.7, metal height of 15–20 cm and anode-cathode distance (ACD) of 4–4.5 cm.

Keywords: Aluminum electrolysis cell, sidewall ledge, Renewable energy consumption, Physical field simulation.

1. Introduction

Aluminum electrolysis as a highly energy-intensive industry, it is not only a highly complex electrochemical process but also faces issues such as outdated production technology, high energy consumption, low production efficiency, and severe pollution. With the global energy revolution, particularly the rapid development of renewable energy, new energy sources have shown promising potential for industrial applications [1]. However, integrating volatile and intermittent renewable energy (e. g., wind, hydro, and solar power) into aluminum electrolysis—a process requiring stable power to maintain production efficiency and quality —poses a critical challenge [2]. Effectively integrating renewable energy while ensuring stable and efficient aluminum electrolysis production remains a major challenge for the industry. Thus, balancing renewable energy consumption with production stability and energy efficiency remains a key issue for the industry.

In 2009, the Fraunhofer Institute for Systems and Innovation Research in Germany [3] proposed and analyzed the feasibility of demand-side participation in wind power grid regulation. The study suggested that the flexible demands of energy-intensive industries—such as chlor-alkali electrolysis, aluminum electrolysis, and ventilation or cooling systems—should be harnessed to

provide balancing capacity. By enhancing the accuracy of wind power forecasting and leveraging the potential of demand response, it is possible to effectively reduce system balancing costs. Zhang et. al conducted an in-depth exploration of key issues related to the integration of wind power into aluminum electrolysis. Through numerical simulations of typical scenarios, they demonstrated that aluminum electrolysis cells possess high resistance to interference. They proposed a method for allowing nearby aluminum electrolysis plants to directly consumption wind power, aiming to achieve a win-win situation [4]. Jian Xu and colleagues [5], addressing the issue of the uneven geographical distribution of wind energy and load in China, proposed a new method for on-site wind energy consumption for wind power generation. They also introduced a power imbalance online identification method and a system frequency control approach based on the Wide Area Measurement System (WAMS). A report on demand response was jointly issued. The report discussed the feasibility and economic advantages of aluminum electrolysis as a demand-side response, from perspectives including aluminum production background, market structure, regulation services, and grid control. It highlighted that aluminum electrolysis consumes electricity very consistently and causes minimal disturbance to the power system [6]. Additionally, the EnPot heat exchanger technology developed has improved the output and current efficiency of aluminum smelters, while also maintaining the thermal balance of the aluminum electrolysis cells under current variations [7]. Studies show that while grid integration and regulation can help to utilize renewable energy in aluminum electrolysis, its variations may cause production instability and equipment damage. To better understand the impact of renewable energy on electrolysis cells, researchers worldwide have been closely focused on monitoring the dynamic changes in the inner shape of the cell ledge.

The side ledge is an essential component in aluminum electrolysis, playing a crucial role throughout the production process. A well-defined side ledge profile can effectively constrict the aluminum melt surface, leading to a higher and more concentrated current density. It also helps to suppress bath-metal interface instabilities, thereby minimizing losses caused by secondary aluminum reactions. Moreover, the side ledge contributes to the regulation of thermal and material balance within the electrolytic cell through its dynamic melting and solidification behavior [8]. The shape of the side ledge varies under different operating conditions, especially due to disturbances caused by current or thermal variations in the electrolytic cell. Its morphology exhibits significant sensitivity to operational parameters, particularly under current or thermal variations. Mohamed et al. [9] examined ledge formation during cell startup, demonstrating that controlled cryolite ratio (CR) adjustment (from neutral bath to 6 % excess AlF_3, CR=2.53) and temperature management led to ledge stabilization (10 cm thickness) within 12 weeks. A study on cell ledge formation during start-up involved operating an electrolytic cell with a neutral bath, gradually increasing excess AlF_3 (CR = 2.53) to 6 % over 12 weeks. Results showed that CR required tighter control, and early temperature rise was linked to decreasing AlF_3 content. The side ledge stabilized at 10 cm thickness within 4 months. Ran et al. [10] investigated the dynamic changes in the cell ledge and thermal balance under current variations of ±15 %. The results indicated that when the current increased, the melting of the cell ledge primarily occurred in the bath layer, while when the current decreased, remelting occurred in the metal layer. It was also found that installing distributed cooling systems on both sides of the electrolytic cell could stabilize the size of the cell ledge at different locations. Francis et al. [11] found negligible differences (< 1 %) between 2D and 3D models in predicting thermal behavior during ±5 % current variations. Zhang et al. developed a transient thermoelectric coupling model, to study the changes in the cell ledge when the current was increased by 10 %, showing that ≤ 10 % current increases within 2 hours caused minimal ledge deformation, though higher currents induced rapid temperature rises and prolonged recovery times [12]. Subsequently, based on this, a non-iterative method was employed and compared with traditional iterative cycles and industrial practices. The results showed that when the current increased by 2 %, there was little change in the sidewall and heat loss rate. However, when the current increased by 5 %, 8 %, and 10 %, melting occurred at

certain points on the sidewall within 8 hours, and the heat loss rate near the molten region of the sidewall changed the more rapidly [13].

To maintain thermal balance during the consumption absorption of renewable energy in electrolytic cells, it is essential not only to understand the patterns of cell ledge shape changes but also to investigate the effects of materials, structure, and processes on thermal balance. Lu et al. [14] conducted structural optimization of lining configurations in ultra-large electrolytic cells, demonstrating that their improved design promoted more uniform thermoelectric field distribution. This enhancement led to superior heat dissipation control, optimal temperature maintenance, balanced sidewall thickness, and improved cell cavity geometry. Ivanova et al. [15] developed a device to study the dynamic behavior of the cell ledge; they investigated the relationship between dynamic changes in the cell ledge and the lining material. Gupta et al. [16] studied the impact of the side wedge-shaped carbon block lining on the cell ledge in an 86-kA aluminum electrolytic cell. The results showed that that near-vertical carbon block configurations demonstrate superior adaptability to current increase compared to traditional designs.

In summary, current understanding remains limited regarding both the operational behavior and consumption capacity of aluminum electrolysis cells under unstable renewable energy inputs. To address these issues, this study establishes a transient electro-thermal strongly coupled solidification model for aluminum electrolytic cells, investigating the thermal balance instability problem caused by current variations during renewable energy consumption. Different inputs of current variations were designed, and the distribution of the temperature field and changes in the shape of the cell ledge were studied. The influence mechanism of various process parameters on the shape of the cell ledge was explored, and a control strategy for current variations was proposed. Ultimately, this study clarifies the process adjustment measures for consuming large-scale current variations in aluminum electrolytic cells, providing theoretical support for the integration of unstable renewable energy into aluminum electrolysis.

1.1 Electro-Thermal Field Strong Coupling Solidification Model

In this study, an electro-thermal field strongly coupled solidification slice model for a 420-kA aluminum electrolytic cell is established, considering the effects of electric field, thermal field, and cell ledge phase change on the temperature distribution and shape of the cell ledge. First, a high-strength direct current is applied to the anode busbar boundary at the top of the aluminum electrolytic cell to solve for the electric field distribution. The current flowing through the conductive parts generates Joule heat due to resistance, thus achieving the strong coupling of the electric and thermal fields. Additionally, the phase change of the cell ledge, induced by changes in the thermal field distribution, is calculated using a solidification-melting model. The phase change of the cell ledge, in turn, affects the electro-thermal field distribution within the electrolytic cell.

1.1.1 Computational Principles and Mathematical Model

The model achieves the coupled calculation of the electric field, energy field, and solidification-melting mathematical models through the ANSYS Fluent simulation platform. Direct current is first supplied to the aluminum electrolytic cell via the anode busbar, flowing through the steel yoke, anode carbon blocks, bath, aluminum liquid, and cathode carbon blocks, and exits through the cathode collector bars, forming a stable electric field distribution within the cell. In Fluent, the calculation of the electric field model is implemented using the following Poisson equation (1) and Ohm's law (2):

$$\nabla\left(\sigma\nabla\varphi\right)+\frac{\rho_e}{\varepsilon_0}=0 \tag{1}$$

$$J=-\sigma\nabla\varphi \tag{2}$$

where:
σ Electrical conductivity of the solid region or the ionic conductivity of the liquid region, S/m
φ Electric potential, V
ρ Charge density, C/m^3
ε_0 Permittivity of free space, F/m
J Current density, A/m^2.

In the model presented in this paper, there is no distribution of point charge, i.e., $\rho_e = 0$. Therefore, Equation (1) can be transformed into the Laplace equation for the electric potential in a source-free region, which is expanded into the three-dimensional conductive differential equation as shown in Equation (3).

$$\frac{\partial}{\partial x}\left(\sigma_x\frac{\partial_\varphi}{\partial x}\right)+\frac{\partial}{\partial y}\left(\sigma_y\frac{\partial_\varphi}{\partial y}\right)+\frac{\partial}{\partial z}\left(\sigma_z\frac{\partial_\varphi}{\partial z}\right)=0 \tag{3}$$

where σ_x, σ_y, σ_z are electrical conductivities of the conductive medium in the X, Y, and Z directions of their coordinate system.

In this study, based on the electro-thermal field, a solidification-melting model for the molten zone is introduced, and the enthalpy (H) - porosity (β) method is used to solve the phase change between the molten zone and the cell ledge in the electrolytic cell [17]. Porosity is introduced to track the solidification-melting interface. When the region is in the solid phase, the liquid fraction is set to 0; when the region is in the liquid phase, the liquid fraction is set to 1; and when the region is in the mushy zone, the liquid fraction is set between 0 and 1.

$$\beta=\begin{cases}0 & T<T_S\\ \frac{T-T_S}{T_L-T_S} & T_S\le T\le T_L\\ 1 & T>T_L\end{cases} \tag{4}$$

where:
β Liquid fraction (porosity), dimensionless
T_S Solidus temperature, K
T_L Liquidus temperature, K.

This study uses the enthalpy method to calculate latent heat, where the total enthalpy H is the sum of the sensible enthalpy h and latent heat ΔH, as shown in Equations (5–7):

$$H=h+\Delta H \tag{5}$$

$$h=h_{ref}+\int_{T_{ref}}^{T}C_P dT \tag{6}$$

$$\Delta H = \beta L \tag{7}$$

where:

h_{ref} Reference enthalpy, J/kg
T_{ref} Reference temperature, 298 K
C_P Specific heat capacity at constant pressure, J/kg·K
L Latent heat of solidification of the molten material, J/kg.

This study also considers the impact of heat sources and heat sinks in the actual electrolytic process on the thermal field, represented by the energy balance equation, Joule's law, and the reaction heat source equation, as shown in Equations (8–10).

$$\frac{\partial}{\partial_t}\left(\rho H\right) = \nabla\left(k\nabla T\right) + S_J + S_a \tag{8}$$

$$S_J = \sigma\left|\nabla\varphi\right|^2 \tag{9}$$

$$S_a = \left(2.124\eta - E_r - E_g\right)I \tag{10}$$

where:

ρ Density, kg/m³
T Temperature, K
k Effective thermal conductivity, W/m·K
S_J Volumetric Joule heat generation, W/m³
S_a Heat of reaction, W/m³
η Current efficiency, dimensionless
E_r Reaction voltage drop, V
E_g Bubble layer voltage drop, V
I Current, A.

1.1.2 Physical Model and Boundary Conditions

To enable rapid and precise prediction of the side ledge shape under current variation, a slice model of a 420-kA cell was established as shown in Figure 1. The model features a conventional carbon block side lining around the molten zone, with a two-layer structure comprising upper bath and lower liquid aluminum phases.

The slice model calculations for the aluminum electrolysis cell under current variations were initialized using steady-state results as the baseline. Typically, to obtain the time-dependent evolution of the solid phase volume fraction in the molten zone, transient simulations were performed by dynamically adjusting the input current density. This approach ensures accurate representation of the electro-thermal coupling during phase transitions under dynamic current conditions [18, 19]. The model accounts for temperature-dependent properties in all conductive regions, including the molten zone, where material behavior is defined by a piecewise function bifurcated at the solid-liquid phase transition temperature. Below the solidus temperature, the electrical conductivity is 1×10^{-8} S/m and the thermal conductivity is 1.69 W/m·K, corresponding to the material properties of the side ledge. Above the liquidus temperature, the thermal conductivity is 1×10^{5} W/m·K and the electrical conductivity is 228.55 S/m. The material properties of the molten zone used in this study are shown in Table 1.

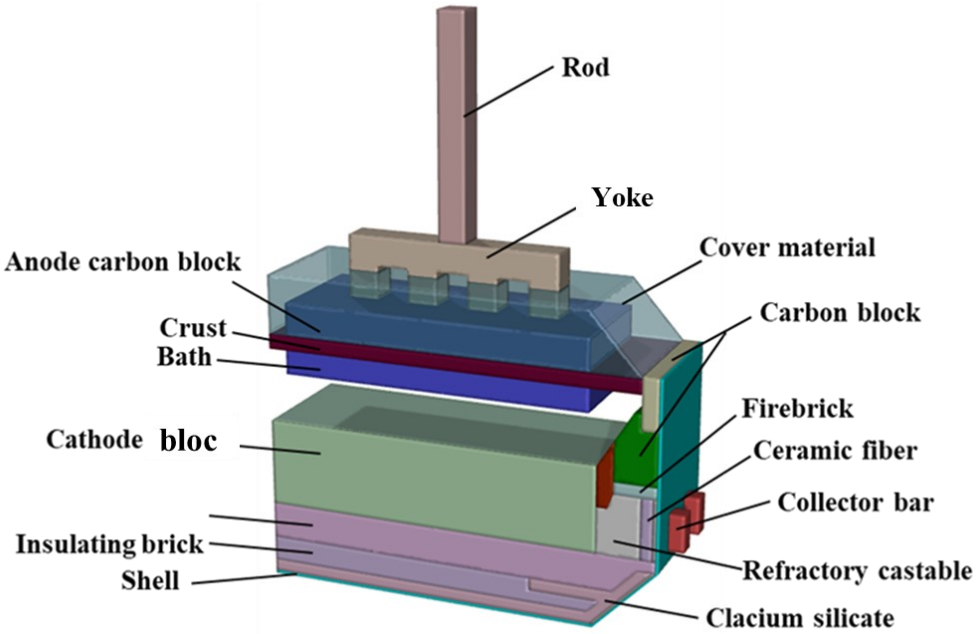

Figure 1. Slice model of a 420-kA aluminium electrolytic cell.

Table 1. Physical parameters of the molten bath and metal.

Physical Parameter	Value	Physical Parameter	Value
Density of bath (kg/m^3)	2130	Electrical conductivity of liquid aluminum (S/m)	3 448 276
Density of liquid aluminum (kg/m^3)	2270	Fusion enthalpy of bath (kJ/kg)	420
Specific heat capacity of bath (J/kg·K)	1660	Fusion enthalpy of aluminum (kJ/kg)	397
Specific heat capacity of liquid aluminum (J/kg·K)	1088	Solidus temperature of bath (°C)	938
Electrical conductivity of bath (S/m)	228.55	Liquidus temperature of bath (°C)	940

Boundary conditions in the Fluent software package mainly include electric field boundary and thermal field boundary conditions. When setting the electric field boundary, a fixed current density is applied at the top of the anode busbar, and the electric potential is set to 0 at the surface of the cathode collector bar end. In setting the thermal field boundary conditions, both convection and radiation are considered, and these are integrated into an equivalent heat transfer coefficient. The fitting relationship between the equivalent heat transfer coefficient and temperature is shown in Table 2. Based on actual production measurements, the environmental temperatures at the top, sides, and bottom of the cell are set to 160 °C, 40 °C, and 38 °C, respectively.

Mesh generation is a pivotal step in finite element simulations, where a balance must be struck between computational accuracy and efficiency. The computational platform used in this study is Fluent, and the mesh generation was performed using the Workbench Mesh module, which is highly compatible with Fluent. To improve mesh quality, a non-integral mesh division was adopted, with regional subdivision based on the defined blocks. The mesh was refined, and after independence verification, the optimized mesh contained a total of 8.07 million cells, with the

maximum aspect ratio of the mesh reduced to 0.84. The resulting discretized model after mesh generation is shown in Figure 2.

Table 2. The relationship between the equivalent heat transfer coefficient of the electrolytic cell boundary and the environment). T is surface temperature in °C.

Thermal field boundary	Heat transfer coefficient (W/(m²·K)
Anode-yoke	3.474 + 0.0946·T
Anode cover material	4.636 + 0.0626·T
Side-shell	7.884 + 0.0936·T
Bottom-shell	9.849 + 0.0651·T

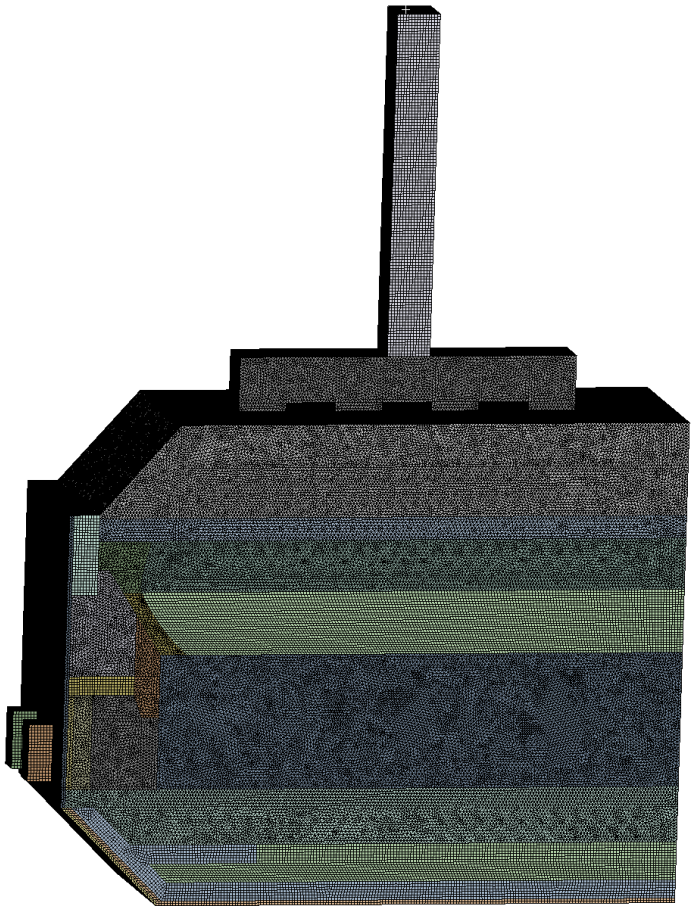

Figure 2. Mesh model of a 420-kA aluminium electrolysis cell.

2. Simulation Results and Analysis

2.1 Analysis of Cell Ledge Shape Changes under Current Changes in the Electrolysis Cell

2.1.1 Changes in Cell Ledge Shape Under Current Increase

In the context of renewable energy consumption, current variations exhibit bidirectional variability (±Δ %) with wide amplitude ranges and prolonged durations. Therefore, this study selected four current variation scenarios: ±5 %, ±10 %, ±15 %, and ±20 % for transient calculations. The duration was selected as it approaches thermal equilibrium, with near-complete ledge melting observed by the 10 h mark in case b, for example (Figure 3).

The cell ledge shape under steady-state current conditions is represented by the black line at 0 hours in the figure. From that last, it is evident that the shape of the cell ledge is generally irregular, with a stepped interface between the liquid bath and aluminum. After a certain period of current increase, the toe (lower part) of the cell ledge begins to melt first, and the lining is eroded. This is primarily due to the thinner side lining in the bath region compared to the molten aluminum region, leading to stronger heat dissipation in the bath zone. From Figure 3(a), it can be observed that when the current increases by 5 % and lasts for 10 hours, the change in cell ledge thickness is not significant. Since the material properties of the molten zone in this study are based on industrial practice, with the molten zone divided into two layers, and the bath being the primary heat generation area, when the current increases by a small range, the upper part of the cell ledge melts more noticeably, with a melting of 7.5 cm within 10 hours. Additionally, the time scale of the shape change in the cell ledge differs. For a 15 % increase over 5 hours, the cell ledge faces the risk of red furnace conditions, while at a 20 % increase, the bottom of the toe melts completely within 2 hours. For current increases of 10 % and above, the gradient of the decrease in cell ledge thickness shows different time inflection points. The time inflection points corresponding to 10 %, 15 %, and 20 % current increases are 6 hours, 3 hours, and 1.5 hours, respectively. Beyond these time inflection points, the gradient of the decrease in cell ledge thickness increases rapidly with time. However, the common pattern is that the cell ledge uniformly thins in the early stages and melts rapidly in the later stages at the metal level. Therefore, when consuming fluctuating renewable energy, appropriate response measures can be taken within the corresponding time inflection points for different ranges of current increase.

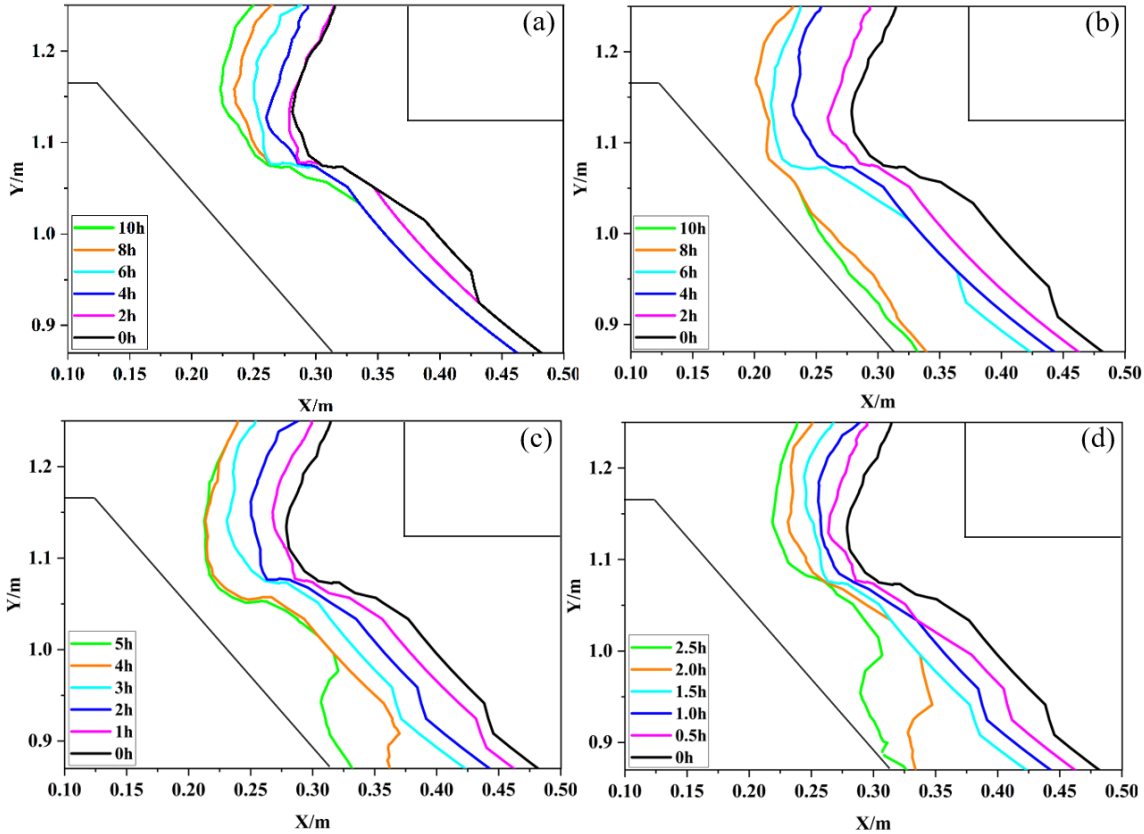

Figure 3. Changes in the shape of the side ledge over time under different current increases. (a): +5 %, (b): +10 %, (c): +15 %, (d): +20 %.

Figure 4 illustrates the changes in the side ledge profile under different current increases (after 2 and 3 h). During current increase, the cell ledge first melts at the toe region. As current increases further, ledge thinning accelerates nonlinearly, with distinct morphological stages. At 15 %

current increase, the decrease in cell ledge thickness is relatively regular over a short period, with an average reduction of approximately 2.5 cm per 5 %, and the change in the aluminum-liquid interface thickness is minimal. The thickness reduction is more significant at the upper and lower parts of the cell ledge. For current increase of 20 % and above, the cell ledge initially melts at the lower toe region, with a reduction of approximately 15 cm within 2 hours. Therefore, with a 15 % current increase, there is a sufficient time window to implement control measures for the electrolytic cell. However, for current increase of 20 % and above, the melting of the side ledge occurs more rapidly, increasing the risk of red potshells and erosion of the cell lining.

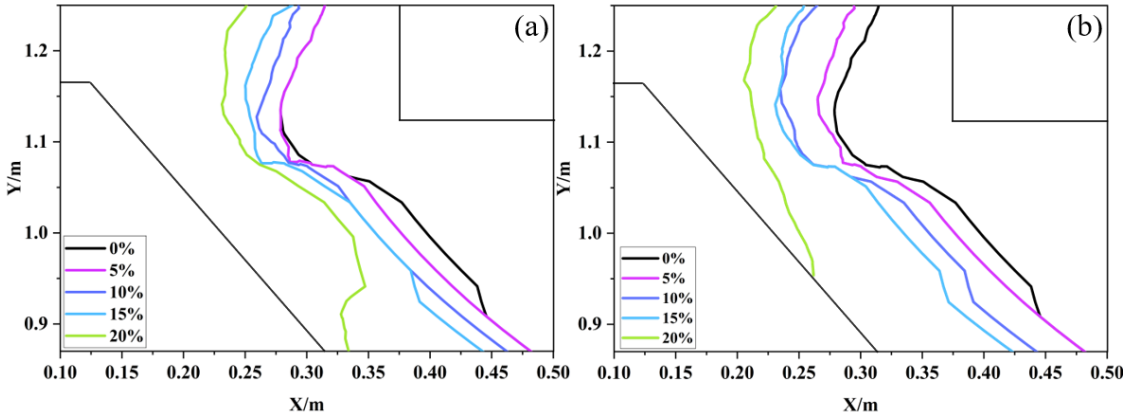

Figure 4. Changes in the shape of the side ledge with current increase. (a): 2 hours, (b): 3 hours.

To investigate the changes in the cell ledge under long-term current variations, Figure 5 shows the evolution of the solid-phase volume in the molten zone over a 10-h transient simulation, which reflects the solidification and melting of the cell ledge. When the current increases by 10 %, the cell ledge volume decreases gradually during 6–7 hours, due to the substantial heat generation overwhelming the melting process, leading to accelerated ledge melting. When the current increases by 10 % or more, the side ledge volume decreases to below 0.02 m^3 within 10 hours, requiring immediate corrective actions. In contrast, variations within ±5 % only result in a minor volume reduction of approximately 0.01 m^3, demonstrating the cell's inherent self-balancing capability for small disturbances. When the current increase is 20 %, the cell ledge volume decreases to below 0.02 m^3 within 2 hours, highlighting the system's vulnerability to severe current variations. The delayed response of process adjustments further exacerbates these challenges, making it impractical to rely solely on the cell's self-regulation for large-scale current variations. These findings underscore the need for proactive control measures when dealing with current variations exceeding ±10 %, particularly to prevent rapid ledge deterioration and potential cell damaging conditions.

Figure 6 presents the temporal temperature evolution at monitoring point (1.08, 1.11, 0.19) beneath the anode carbon block under four current increase scenarios (5 %, 10 %, 15 %, 20 %). The temperature profiles exhibit characteristic transient behavior: an initial rapid heating phase followed by thermal stabilization, with the heating rate directly correlated to current increase. At a 20 % current increase, the temperature increases from 948.75 °C to 960 °C within 1.5 hours, a rise of 11.25 °C. Due to the presence of latent heat during melting, the temperature increase curve fluctuates continuously before ultimately stabilizing. The system ultimately reaches equilibrium temperatures of 953 °C, 955 °C, 958 °C, and 960 °C for 5 %, 10 %, 15 %, and 20 % current increase respectively, demonstrating a maximum thermal overshoot of approximately 12 °C beyond baseline conditions.

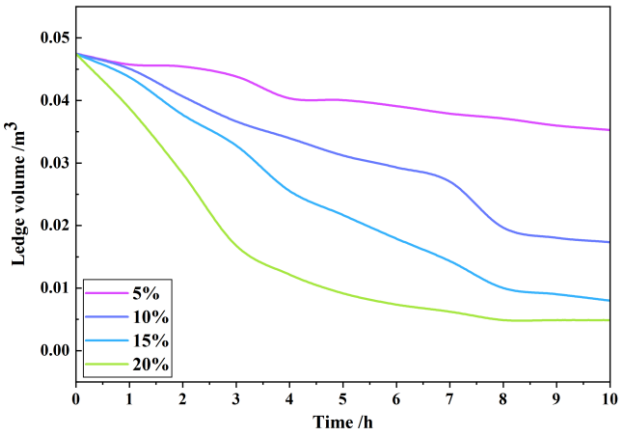

Figure 5. Changes in cell ledge volume over time under current increase.

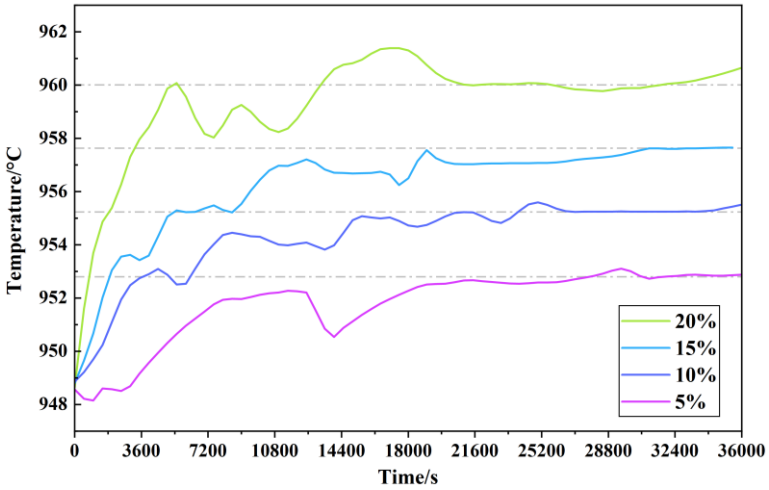

Figure 6. Variation of bath temperature with time as current increases.

2.1.2 The Effect of Bath Height

Figure 7 demonstrates the evolution of side ledge morphology under current reduction (-5 to -20 %) over a 10-h period. When the current is reduced by 5 % for 10 hours, the change in cell ledge thickness is minimal, indicating that the cell has some self-regulating capability within the ±5 % variation. For current reduction up to 15 %, the rate of thickening of the cell ledge toe is relatively uniform. However, when the current is reduced by 20 %, the toe thickens more rapidly, and the thickness increases at an accelerating rate over time. As shown in Figure 7 (d), between 6 and 8 hours, the toe thickness increases at a rate of 2.5 cm/h, and between 8 and 10 hours, the rate increases to 7.5 cm/h, with an overall increase of approximately 32.5 cm within 10 hours. The ledge develops non-uniformly during current reduction, with preferential thickening at the toe and bulging toward the bath zone. Compared to the situation with current increase, when the current decreases, the rate of increase in the ledge thickness at different molten zone depths is different. The shape of the cell ledge becomes uneven, possibly due to increased liquid aluminum instabilities caused by the thickening of the ledge toe. Furthermore, compared to risk associated with the cell in overheated condition with significant current increase, a substantial current decrease does not erode the cell lining, but it increases the risk if sludge formation at the bottom of cell cavity, which leads to uneven cathode current distribution, causing magnetic field disturbances. These effects increase bath-metal interface instabilities and voltage oscillations, potentially leading to uneven anode current distribution and anode burn-off risks.

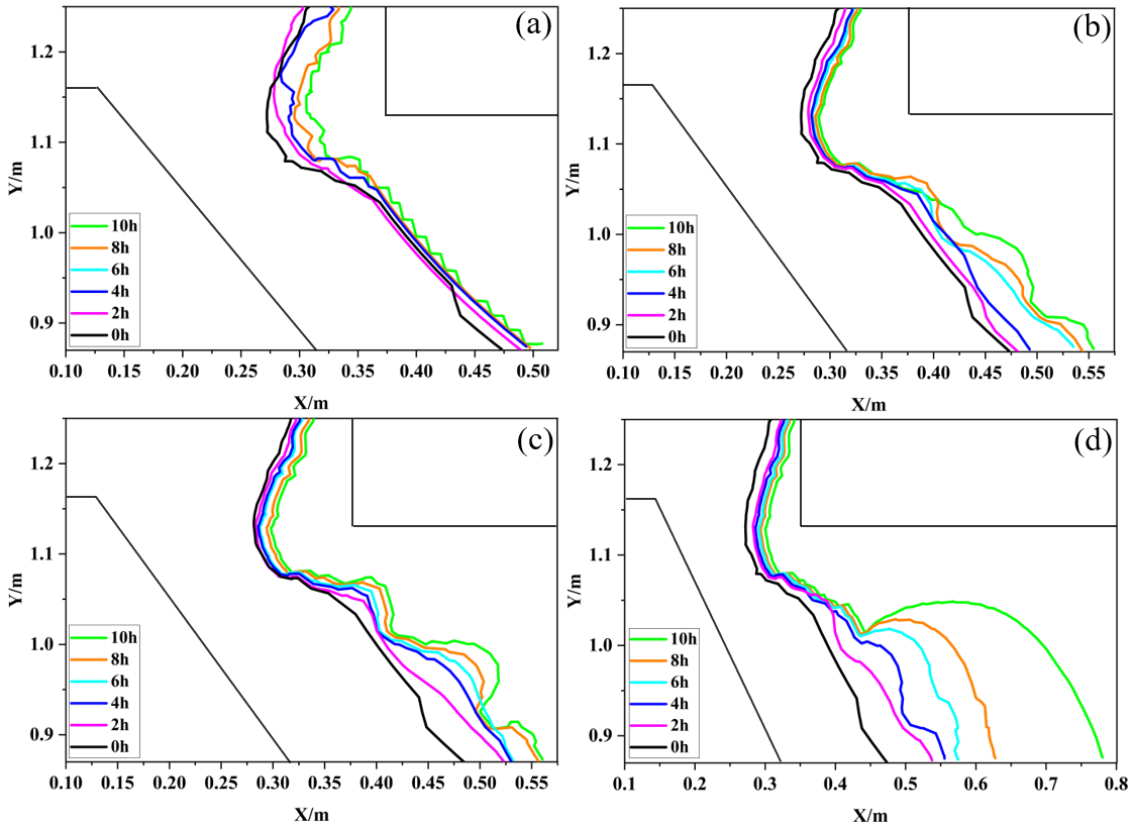

Figure 7. Changes in the shape of the cell ledge with current reduction. (a): -5 %, (b): -10 %, (c): -15 %, (d): -20 %.

Figure 8 illustrates the evolving liquid phase volume fraction distribution in the molten zone during sustained 20 % current reduction, revealing distinct solidification patterns. With a significant current reduction and constant heat dissipation, the overall heat generation decreases, and the bath temperature first decreases at the solid-liquid interface. From the color changes and distribution areas in Figure 8, it can be observed that as the variation time increases, the red region gradually shrinks, meaning the area with a liquid phase volume fraction of 1 decreases, while the area with a volume fraction between 0 and 1 increases. The mushy zone near the bottom toe of the cell bulges first, gradually becoming thicker and wider, eventually solidifying into a solid cell ledge.

Figure 9 presents the quantitative evolution of side ledge volume under current reduction, revealing three distinct operational regimes. When the current reduction is within 10 %, the cell ledge volume changes by 0.02 m^3, indicating the effectiveness of the installed sidewall insulation in maintaining thermal equilibrium. When the current reduction reaches 15 % or more, a marked thermal transition occurs where the ledge volume increases at an accelerating rate. Excessive thickening of the cell ledge severely impacts the distribution of the multi-field electromagnetic flow within the cell.

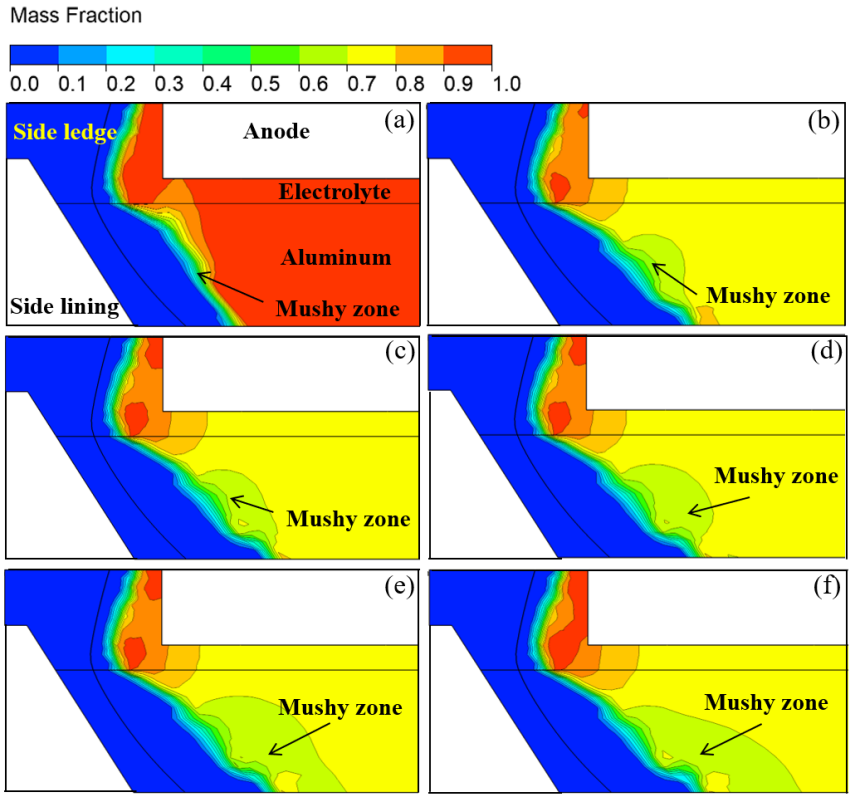

Figure 8. Changes in the cell ledge shape over time under a 20 % current reduction. (a): 1 h, (b): 3 h, (c): 5 h, (d): 7 h, (e): 9 h, (f): 11 h.

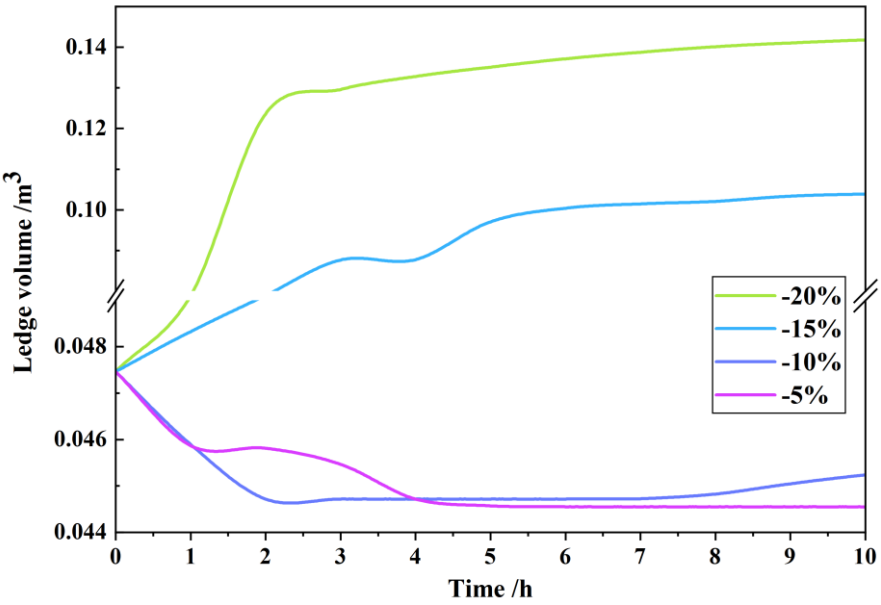

Figure 9. Variation of cell ledge volume with time under current reduction.

The temperature variation beneath the anode carbon block in the bath region under current reduction is shown in Figure 10. When the current decreases by 5 %, the system exhibits oscillatory behavior: an initial temperature drop is followed by a rebound to 953 °C at 4 hours due to latent heat release during ledge solidification, then stabilizes at 950 °C after 6 hours as heat generation and dissipation reach equilibrium. When the current decreases by 10 %, the temperature rises to a peak of 952.7 °C within 1.5 hours and then decreases, stabilizing at 943 °C

after 9 hours. With a significant current reduction and a slow self-balancing process of the cell ledge, the temperature quickly drops to the minimum value. When the current decreases by 15 %, the temperature drops to the initial crystallization temperature line (940 °C within 2 hours and stabilizes. For a 20 % reduction, the temperature drops below the initial crystallization temperature line within 1 h and stabilizes. The aluminum electrolytic cell experiences a cold cell phenomenon in a short period. Therefore, the traditional aluminum electrolytic cell cannot adapt to current reductions of more than 15 %.

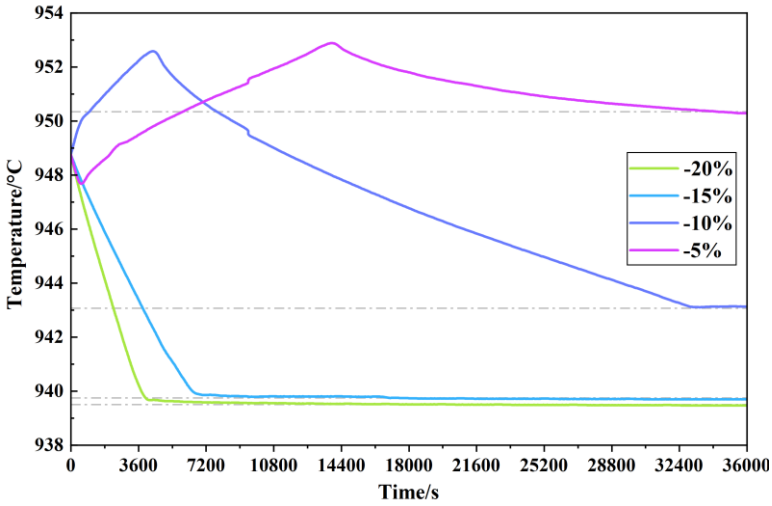

Figure 10. Variation of bath temperature with time under current reduction.

2.2 The Impact of Different Process Parameters on the Shape of the Cell Ledge

In the electrolytic production process, relevant process parameters also play a crucial role in the performance of the electrolytic cell. To enhance the aluminum electrolytic cell adaptability to current variations, this study investigates the effects of bath composition, bath height, and ACD and anode cover material on the cell ledge profile. All results are derived from transient calculations, with a time step set to 0.1 seconds.

2.2.1 The Effect of Bath Composition

The bath is primarily composed of cryolite (Na_3AlF_6), alumina (Al_2O_3), and other salt additives (such as AlF_3, CaF_2, MgF_2, LiF). The formation of the cell ledge is closely related to bath composition. In industrial production, the bath composition is adjusted via computer-controlled dosing to ensure that properties such as the initial crystallization temperature, density, electrical conductivity, and viscosity remain within acceptable ranges, thereby maintaining the thermal balance and current efficiency of the electrolytic cell. This section investigates the effects of the molecular ratio, MgF_2, CaF_2, and Al_2O_3 concentrations on the shape of the cell ledge.

Five equidistant points were selected within the conventional molecular ratio range: 2.1, 2.3, 2.5, 2.7, and 2.9. Figure 11 illustrates the effect of the molecular ratio on the shape of the cell ledge. As the molecular ratio increases, the cell ledge becomes thicker. When the molecular ratio is 2.1, the cell ledge toe is relatively thin, while at a molecular ratio of 2.9, the toe becomes thicker and extends directly above the cathode carbon block, affecting the magnetic field distribution within the electrolytic cell. Therefore, a molecular ratio range of 2.3 to 2.7 is considered more appropriate.

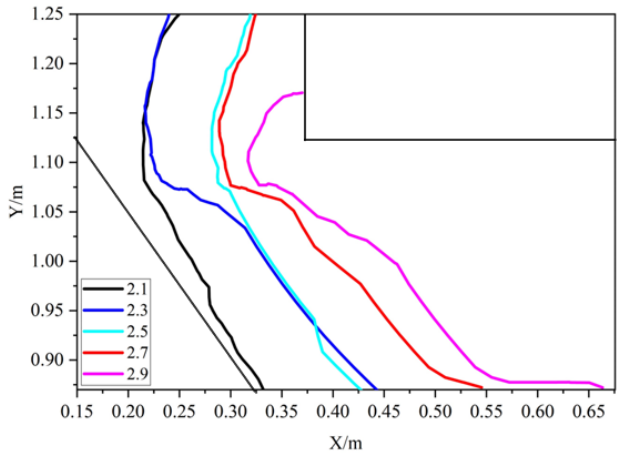

Figure 11. The shape of the cell ledge as a function of molecular ratio.

Four distinct mass fractions of MgF_2 (0.5 %, 1.5 %, 2.5 %, and 3.5 %) were selected to investigate their effects on the morphological characteristics of the side ledge. Figure 12 shows the effect of different mass fractions of MgF_2 on the shape of the cell ledge. The mass fraction of MgF_2 exhibits a significant inverse correlation with the ledge thickness. When the mass fraction is less than 1.5 %, the cell ledge toe is relatively thick. When the mass fraction is between 2.5 and 3.5 %, the thickness of the cell ledge is more reasonable. Furthermore, the mass fraction of MgF_2 plays a critical role in determining the ledge formation dynamics, wherein a reduction in MgF_2 concentration directly correlates with an increase in ledge length.

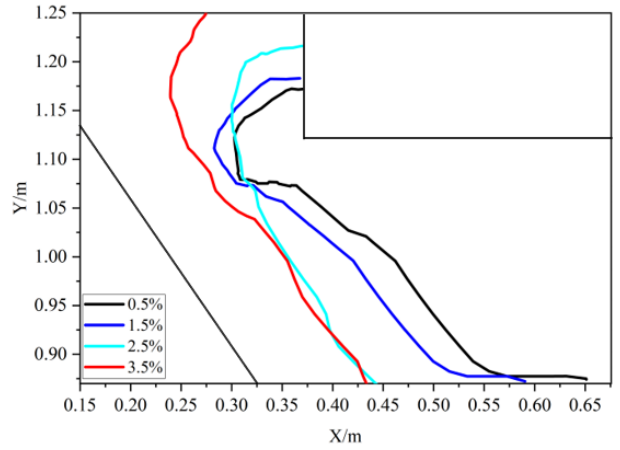

Figure 12. The shape of the side ledge as a function of MgF_2 mass fraction.

Five discrete mass fractions of CaF_2 (0 %, 2 %, 4 %, 6 %, and 8 %) were examined to assess their influence on cell ledge morphology. As depicted in Figure 13, an increase in CaF_2 concentration leads to a gradual thinning of the cell ledge. Within the range of 0 to 8 %, the thickness of the cell ledge toe does not show signs of being too thick or too thin. The bath region corresponds to a greater change in cell ledge thickness. When the CaF_2 concentration falls below 2 %, the upper part of the electrolytic cell becomes overcooled, and the upper cell ledge comes into contact with the anode carbon block. Therefore, it is recommended to maintain the CaF_2 mass fraction within the range of 4 to 8 % in industrial practice. This range allows for effective control over the upper ledge thickness by modulating CaF_2 addition.

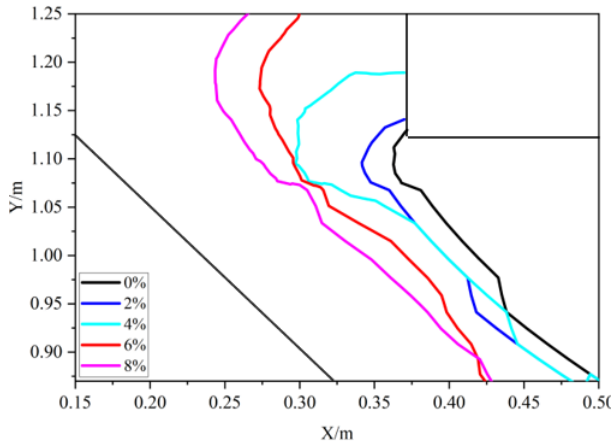

Figure 13. The shape of the cell ledge as a function of CaF_2 mass fraction.

Based on the conventional range of Al_2O_3, mass fractions of 1.5 %, 2 %, 2.5 %, and 3.5 % were selected. Figure 14 shows the changes in the shape of the electrolytic cell ledge at different Al_2O_3 mass fractions: The mass fraction of Al_2O_3 is negatively correlated with the thickness of the cell ledge. Specifically, at 1.5 % Al_2O_3, the upper ledge displays a pronounced thickening, whereas within the 2–3 % range, the upper ledge thickness stabilizes. While reducing alumina content can effectively increase ledge thickness, caution must be exercised to avoid excessively low concentrations, as this may trigger the anode effect.

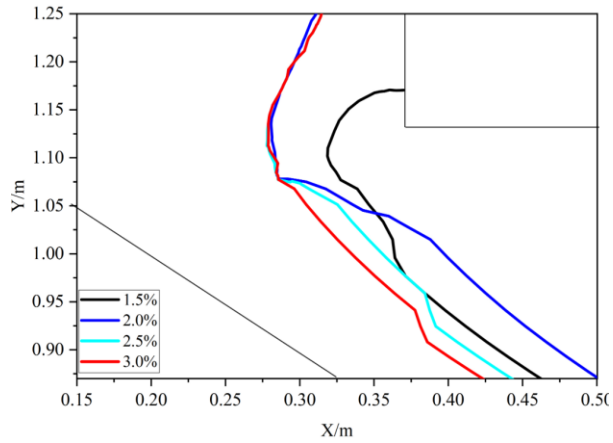

Figure 14. The shape of the cell ledge as a function of Al_2O_3 mass fraction.

2.2.2 The Effect of Bath Height

To investigate the effect bath height on cell ledge morphology, the height of the cell cavity was kept constant at 40 cm while maintaining constant input parameters. The ratio of bath to molten aluminum in the liquid phase was varied by adjusting the bath height to 10 cm, 15 cm, 20 cm, 22 cm, and 25 cm, corresponding to the aluminum height of 30 cm, 25 cm, 20 cm, 18 cm, and 15 cm, respectively, while maintaining the ACD at 4.5 cm. The results are shown in Figure 15.

As the ratio of bath height to molten aluminum height in the liquid phase of the cell increases, the maximum bath temperature initially decreases and then increases. A 5-cm change in the bath height results in a temperature change of approximately 10 °C. Both excessively high and low bath height lead to an increase in bath temperature and a decrease in cell ledge thickness. When the bath height is around 20 cm (i. e., the ratio of bath to aluminum height is 1), the cell ledge thickness is more appropriate. As shown in Figure 15, when the bath height changes, the change

in the cell ledge toe is not significant, but the change in the thickness of the cell ledge corresponding to the bath region is more pronounced. In conclusion, the simulations show that the bath height of 20–25 cm and the metal height of 15–20 cm, will allow a stable bath temperature and cell ledge when facing current variations. However, in industrial practice, it is more common to have bath height of 16–19 cm and metal height of 20–25 cm.

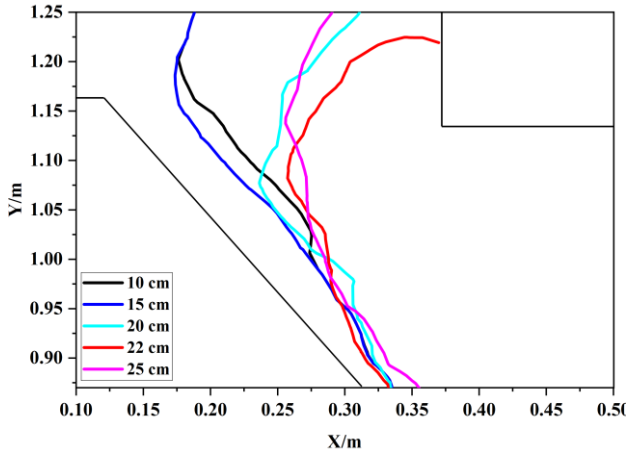

Figure 15. Shape of the cell ledge as a function of bath height.

2.2.3 The Effect of ACD

To investigate the effect of anode distance on the shape of the cell ledge, five different anode distances were selected: 3.5 cm, 4.0 cm, 4.5 cm, 5.0 cm, and 5.5 cm. Under constant bath and metal height and material properties, and inner lining structure, the influence of ACD on the shape of the cell ledge was studied. The calculation results are shown in Figure 16. When the anode cathode distance is 3.5 cm, the cell ledge is thicker, and the toe extends to the middle of the liquid phase, affecting the normal operation of the electrolytic cell. When the anode cathode distance exceeds 5 cm, the cell ledge has almost no toe, which can erode the cell lining. An anode distance between 4 and 4.5 cm is more appropriate. Under fluctuating renewable energy currents, the cell ledge thickness can be increased by reducing the ACD (if there is room for ACD reduction considering magnetic stability circumstances), thereby enhancing the thermal insulation performance of the electrolysis cell.

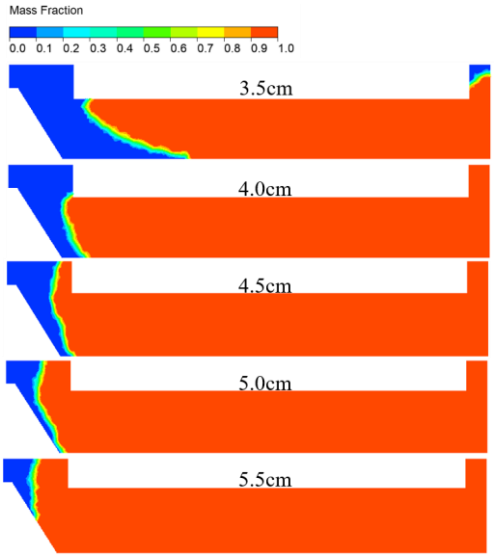

Figure 16. The shape of the cell ledge as a function of ACD.

2.3 Process Adjustment Strategy for Cells Under Current Variations

Based on computational simulations of the steady-state temperature field and heat dissipation distribution in 420-kA cells under standard current conditions, the top three sources of heat dissipation in the electrolytic cell are the potshell at the molten zone (bath and metal), top anode cover material, and anode steel yoke, with the cathode collector bars and anode rods following. Among these, the heat dissipation from the potshell at the level of molten zone (bath and metal) accounts for the largest proportion. On one hand, the most direct factors influencing the heat dissipation from the cell sides are the thermal insulation and heat dissipation performance and stability of different inner side-lining structures. On the other hand, without changing the cell structure, the side heat dissipation can be adjusted by modifying the cell ledge thickness, which is related to process parameters such as bath composition, bath temperature, ACD, and metal height. The anode-cover material and anode steel yoke both contribute to top heat dissipation. The heat dissipation from the anode-cover material is mainly adjusted by changing its thickness, which also changes the heat loss from the yoke. Based on the previous computational analysis of the changes in the cell ledge under large current variations, as well as the mechanistic effects of electrolytic process parameters and cell structural configurations on ledge formation, this paper summarizes the process adjustment strategies for traditional cells operating with varying renewable energy currents.

1) The adaptability of traditional cells to large-scale current variations: Present electrolysis cells have a certain self-regulation capability within the ±5 % current variation. When the current increases by 10 % or 15 %, the time inflection points for the decrease of the cell ledge thickness is 6 hours and 3 hours, respectively. Beyond these time inflection points, the decrease in cell ledge thickness accelerates rapidly, requiring timely response. When the current is reduced by 10 %, the changes in the cell ledge are not significant, and the cell cooling is relatively small, the corresponding measures should be taken within 9 hours. When the current is reduced by 15 % or more, bath temperature rapidly drops below the solidus temperature; in this case, increasing of cell ledge thickness does not provide enough thermal insulation rapidly enough to prevent the bath temperature drop. Similarly, when the current increases by 20 %, the cell ledge volume decreases to below 0.02 m^3 within 2 hours. Therefore, it is difficult to operate the cell under large-scale changes of the current solely through the self-balancing of the electrolytic cell and related process control measures.

2) Among the operational parameters of the cell, changes in the ACD, molar ratio, and the metal height have a significant impact on the thickness of the cell ledge. Therefore, when the input current variation in the aluminum electrolytic cell is large, process adjustments such as raising or lowering the anode beam (increasing or decreasing ACD), amount of aluminum tapping, alumina feeding rate, and adjustment of the flue gas flow rate can be used to control the thermal balance of the cell. When the current variation exceeds the self-balancing capacity of the cell there is enough time to adjust bath additives such as MgF_2, CaF_2, and Al_2O_3 in the bath. For long-term current changes, the thickness of the anode cover material can also be adjusted.

3. Conclusions

This study investigates current variation challenges (up to ±20 %) in 420-kA aluminum electrolysis cells during renewable energy consumption. By establishing a coupled electro-thermal solidification model, we systematically analyzed ledge morphology evolution under various current variations and process parameters. The findings provide theoretical guidance for stable operation during substantial consumption of renewable energy.

The main conclusions of this study are as follows:

(1) Based on the transient electro-thermal strongly coupled solidification model of the cell, the temperature field distribution and cell ledge shape changes under ±20 % current variations were studied. The results show that during current variations, the cell ledge first solidifies or melts at the lower (toe) region. The current electrolytic cell has a certain self-regulation ability within the ±5 % variation range. When the current increases by 10 or 15 %, the gradient of the decrease in cell ledge thickness has different time inflection points, occurring at 6 hours and 3 hours, respectively. Beyond these time inflection points, the gradient of the decrease in cell ledge thickness increases rapidly over time. When the current increases by 20 %, the cell ledge volume decreases to below 0.02 m^3 within 2 hours. When the current decreases by 10 %, bath temperature stabilizes at 943 °C after 9 hours. When the current decreases by more than 15 %, bath temperature drops to near the solidus temperature line within 2 hours, causing the cell ledge to bulge upwards and resulting in severe uneven distribution of the shape, which affects the electromagnetic field distribution within the cell and MHD stability.

(2) The influence mechanisms of different process parameters on the shape of the cell ledge were investigated. The ACD, molar ratio, and the height of molten aluminum have significant impact on the cell ledge thickness. Except for the molar ratio, which is directly proportional to the cell ledge thickness, the ACD, the metal height, anode cover material thickness, and concentrations of additives (MgF_2, CaF_2, Al_2O_3) are inversely proportional to the resulting cell ledge thickness.

(3) A control strategy for the cell under current variations is proposed. That is, under current variations, the control is based on the influence mechanisms of different process parameters on the cell ledge, but it must be kept within a reasonable range to prevent extreme conditions such as red potshells or cold cell. Specifically, the recommended ranges are: MgF_2 (2.5–3.5 wt.%), CaF_2 (4–8 wt.%), Al_2O_3 (2–3 wt.%), molecular ratio (2.3–2.7), metal height (15–20 cm) and anode cathode distance (4.0–4.5 cm).

4. Acknowledgments

This work was financially supported by the National Key Research and Development Program of China (No. 2022YFB3304902), the NSFC Joint Fund of China (No. U2202253), the 2023 Cutting-Edge Interdisciplinary Project of Central South University, China (No. 2023QYJC007), Yunnan Province Science and Technology Planning Project of China (No. 202202AB080017) and the Key Fund of the National Natural Science Foundation of China (No. 62133016), and the National Natural Science Foundation of China (NSFC) Young Scientists Fund (No. 52404374)

5. References

1. X.F. Zheng et al., A review of thermoelectrics research – recent developments and potentials for sustainable and renewable energy applications, *Renewable and Sustainable Energy Reviews* 2014, 32, 486–503. https://doi.org/10.1016/j.rser.2013.12.053
2. Feixiang Gong et al., Review of electrolytic aluminum load participating in demand response to absorb new energy potential and methods, *IEEE*, 2021. https://doi.org/10.1109/icbaie52039.2021.9389999
3. Marian Klobasa, Analysis of demand response and wind integration in Germany's electricity market, *IET Renewable Power Generation* 2010, 4(1), 55–63. https://doi.org/10.1049/iet-rpg.2008.0086
4. Hongliang Zhang et al., Analysis and countermeasures of wind power accommodation by aluminum electrolysis pot-lines in China, *Metallurgical and Materials Transactions B* 2017, 48, 2526–2534. https://doi.org/10.1007/s11663-017-1009-6

5. Jian Xu et al., An isolated industrial power system driven by wind-coal power for aluminum productions: a case study of frequency control, *IEEE Transactions on Power Systems* 2014, 30(1), 471–483. https://doi.org/10.1109/tpwrs.2014.2322080
6. D. Tod et al, Michael R. Starke et al., Providing reliability services through demand response: a preliminary evaluation of the demand response capabilities of Alcoa inc., 2009. https://doi.org/10.2172/948544
7. Pascal Lavoie et al., Increasing the power modulation window of aluminium smelter pots with shell heat exchanger technology, *Light Metals* 2011, 369–374. https://doi.org/10.1002/9781118061992.ch66
8. Ling Ran et al., Improved CFD modeling of the whole-cell side ledge behavior in aluminum electrolysis cell, *Metallurgical and Materials Transactions B* 2023, 54(3), 1122–1130. https://doi.org/10.1007/s11663-023-02747-y
9. Mohamed M. Ali et al., Thermal behavior of the early life of an aluminum electrolysis cell, *International Journal of Engineering Research in Africa* 2022, 61, 51–67. https://doi.org/10.4028/p-v5kt07
10. Ling Ran et al., Fully-coupled electric-thermal-flow modeling and investigation of dynamic thermal-ledge behavior in aluminum electrolysis cell, *Journal of The Electrochemical Society* 2024, 171(9), 093507. https://doi.org/10.1149/1945-7111/ad778f
11. Francis Lalancette et al., Dimensional reduction of a 3D thermoelectric model to create a reliable and time-efficient 2D model representing an aluminum electrolysis cell, *International Journal of Heat and Mass Transfer* 2023, 202, 123777. https://doi.org/10.1016/j.ijheatmasstransfer.2022.123777
12. Hongliang Zhang et al., Effect of current transient enhancement on thermal field of aluminum electrolysis cell for the accommodation of wind power, *Journal of Sustainable Metallurgy* 2018, 4, 359–366. https://doi.org/10.1007/s40831-018-0177-1
13. Hongliang Zhang et al., Study on side ledge behavior under current fluctuations based on coupled thermo-electric model, *Light Metals* 2019. https://doi.org/10.1007/978-3-030-05864-7_80
14. Dingxiong Lu et al., Development of NEUI500kA family high energy efficiency aluminum reduction pot ("HEEP") technology, *Light Metals* 2011, 455–460. https://doi.org/10.1002/9781118061992.ch81
15. Anela M. Ivanova et al., Experimental studies of the dynamic formation of the side ledge in an aluminum electrolysis cell, *Russian Metallurgy (Metally)* 2020, 133–137. https://doi.org/10.1134/s0036029520020068
16. Amit Gupta and Sankar Namboothiri, Impact of carbon seam on freeze profile in aluminum reduction cell, *Transactions of the Indian Institute of Metals* 2017, 70, 1563–1574. https://doi.org/10.1007/s12666-016-0954-0
17. Ali C. Kheirabadi and Dominic Groulx, Simulating phase change heat transfer using comsol and fluent: effect of the mushy-zone constant, *Computational Thermal Sciences: An International Journal* 2015, 7(5-6), 427–440. https://doi.org/10.1615/computthermalscien.2016014279
18. Jie Li et al., Design and optimization method of controlled heat exchange structure for aluminum electrolysis cell under current fluctuations, *MetaResource* 2024, 1(1), 23–46.
19. Jinsong Hua et al., Numerical simulation of multiphase magnetohydrodynamic flow and deformation of electrolyte–metal interface in aluminum electrolysis cells, *Metallurgical and Materials Transactions B* 2018, 49, 1246–1266. https://doi.org/10.1007/s11663-018-1190-2
20. Jianfei Zhou and Marc Dupuis, In-depth analysis of lining designs for several 420 kA electrolytic cells, *Light Metals* 2015, 685–690. https://doi.org/10.1007/978-3-319-48248-4_115